RSC Advances

PAPER

View Article Online
View Journal | View Issue

Cite this: *RSC Adv.*, 2026, **16**, 25772

Modelling simple and complex metal-oxide and -hydroxide surface structures using their point of zero charge

Miriam Leffler *[a] and Steven L. Suib [b]

Multiple methods are available to measure organic and inorganic structures in an aqueous environment. These techniques though are mainly used for measuring and modelling the global structures of species in solution, molecules, polymers, biological compounds, and individual structure factors, not surfaces. Since surface structure and composition are directly responsible for a materials point of zero charge it is the ideal property for determining its global structure and composition. Multiple metal-oxides and -hydroxides in an aqueous environment, under varying conditions are also subject to changes in their surface structure and composition. Therefore, this work focuses solely on modelling the global surface structure of simple and complex metal-oxides and –hydroxides in an aqueous environment at their solid/liquid interface, as there are no other methods currently available for this task. The model developed for this work was obtained by augmenting a model originally used for predicting the point of zero charge for both simple and complex metal-oxides and –hydroxides using only their structure factors. To adapt the original model, it was necessary to determine not only each materials set of structure factors but also its surface properties (*i.e.* bond ionic content). The method then developed required a determination of each of the possible stable surface crystal structures at its point of zero charge (pH). Each of these structures was then placed in the model to determine which global structure converged to its experimental point of zero charge.

Received 15th January 2026
Accepted 28th April 2026

DOI: 10.1039/d6ra00388e

rsc.li/rsc-advances

1 Introduction

1.1 The uses of point of zero charge

The importance of a material's point of zero charge (PZC) cannot be overstated as the property is used to determine the attraction between materials. Areas such as flotation[1] use it to assure the adsorption of surfactants to allow the extraction of the components within the ore matrix for collection. In catalysis,[2] it allows the adsorption of a metal catalyst onto its support material. Contact angles and surface energy[3,4] are also affected by this property. PZC is also used in allowing the best conditions for dyeing of clothing.[5] Charge storage methods using activated Carbons in Aqueous Electrolytes[6] also employs this property. While this is only small sample size of this property uses, these examples make it clear its importance.

1.2 Techniques for identification of structures in solution

Determining the structure of both crystalline and amorphous materials in an aqueous solution has been accomplished using multiple techniques. These range from X-ray diffraction and small-angle neutron scattering,[7] Fast Fourier Infrared Spectroscopy,[8] Raman and X-ray Absorption Fine Structure (XAFS) Spectroscopy,[9] to Extended X-ray Absorption Fine Spectroscopy (EXAFS),[10] and Nuclear Magnetic Spectroscopy (NMR).[11] These techniques though are geared toward the identification of species in solution and individual and global structure factors for molecules, polymers, biological compounds, and inorganic particles in an aqueous environment.

It is important to understand the importance of a materials surface structure and composition's effect on its PZC value. Work by Yoon *et al.*,[12] Leffler *et al.*,[13] Lutzenkirchen[14] and Auer *et al.*[15] demonstrated that the surface structure is one of the critical factors responsible for PZC values. Work by Di Paola *et al.*[16] found that changing the surface composition of TiO_2 using different surface dopant atoms, shifted the material's PZC values significantly, while not affecting the global surface structure of the catalyst support (*i.e.* TiO_2). Work by Suchanek *et al.*[17] also demonstrated the same effect of changing the surface composition of 3% yttrium doped zirconia (YSZ) by doping its surface with neodymium (Nd) and gadolinium (Gd). X-ray diffraction patterns demonstrated that the bulk structure remained constant while PZC values of the doped surfaces shifted upwards of 1 pH unit away from the PZC of the undoped YSZ surface. Taken together, these works demonstrate that the

[a]*Department of Chemistry, University of Connecticut, USA. E-mail: Miriamleffler1066@gmail.com*
[b]*Department of Chemistry, Director of IMS Board of Trustees Distinguished Professor University of Connecticut, USA. E-mail: Steven.Suib@uconn.edu*

surface composition and structure at the solid/aqueous interface are the critical factors determining a material's PZC value.

At present none of the available methods for determining the global surface structure and composition of a material can be used in an aqueous environment. It has been demonstrated though that PZC is determined solely by the material's global surface structure and composition at its solid/liquid interface.[12–14,16,17] Therefore, knowledge of a material's PZC value was determined to be ideal for modelling its global surface structure and composition. This was the impetus for developing the augmented model[12] and the new method presented in this work to model the material's global surface structure, composition and properties (*i.e.* bond ionic content) at the solid/aqueous interface using its PZC.

1.3 Structure and composition of the Stern Layer, outer helmholtz layer and diffuse region (general solution) around a metal-oxide surface

When constructing a model, it is critical to understand the physical system under consideration. An examination of the literature on metal-oxide/hydroxide surfaces in an aqueous environment reveals a complex interaction between its surface structure, composition and the makeup of the solution. Therefore, to draw the correct assumptions for a model describing a given system it was imperative to obtain the full understanding of how the entire system functions.

Beginning with Livey and Murray's[18] work on the geometry of solid oxides and carbide surfaces, they determined that oxygen atoms at the surface screen the cations to achieve the lowest possible surface energy. It is accomplished by the oxygen pulling up and over the metal cations. This results in the surface metal cations being situated below the level at which the surface oxygens are located, having retracted downward toward the interior bulk structure.

Work by Leffler *et al.*'s[13] findings support Livey and Murray's[18] surface model. They determined that above a diameter of approximately 29 nm for anatase titania (Region I), the surface structure, PZC, surface charge, and bond ionic content remain constant. In Region I, the surface has the highest measurable PZC value (*i.e.* pH $\cong$ 7.17) of this material. They also determined that electrons transferred to the surrounding oxygen atoms appear to bow back towards the metal cations, acting to partially shield them, in the manner described by Livey and Murray.[18]

Declining particle size below a diameter of approximately 29 nm (Region II), pH_{PZC} values decreased almost linearly with increasing surface bond lengths, indicating that the global percentage of the of the surface which is positive increased significantly. This demonstrated that the metal cations below the oxygen atoms were moving upward toward the surface with decreasing particle size. At a given particle size the metal cations would most likely be situated at approximately the same elevation as the surface oxygen.

Recent work by Brown *et al.*,[19] using a micro-jet, coupled with X-ray Photoelectron Spectroscopy (XPS) determined the structure and composition of the Stern Layer, Outer Helmholtz Plane (OHP) and Diffuse Region (general solution) above silica (SiO_2)

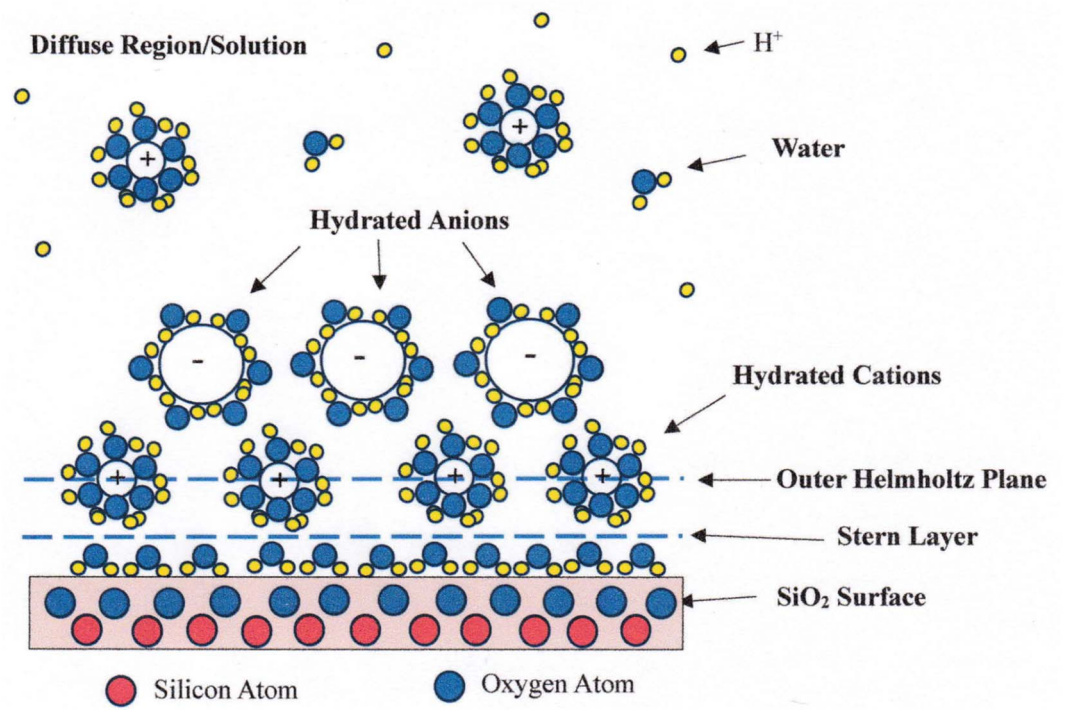

Fig. 1 The structure and composition of the Stern layer, outer Helmholtz plane and diffuse region (general solution) at and above the surface of a silicon dioxide (SiO_2) particle. [After Livey and Murray,[18] and Brown *et al.*[19]]. The positioning of the oxygen to silicon atoms at the surface are in accord with Livey and Murray.[18]

metal-oxide particles [Fig. 1]. Their work focused on how the cations of four different electrolyte solutions, LiCl, NaCl, KCl, and CsCl were located with respect to the Stern layer, OHP and Diffuse Layer (general solution). Lastly, they determined the composition of the diffuse region (general solution).

They determined that the Stern layer was a single layer of water molecules in various orientations with only the hydrogen atoms on the water molecules being adsorbed onto the surface (*i.e.* in contract with). This single layer of water molecules is bounded by the Outer Helmholtz Plane (OHP). At the line defining the OHP layer they identified only hydrated cations from each electrolyte, which would most likely be neutralizing the charge on the oxygen of the adsorbed water molecules. Beyond the OHP, in the diffuse region (general solution) they identified water, hydrated cations and hydrated anions. In addition to Brown *et al.*'s findings,[19] a small amount of water is also known to dissociate into hydroxyls ($O–H^-$) and hydronium ions (H^+)[20] ergo they would also be present in the diffuse region (general solution).

The findings of Brown *et al.*[19] indicated that the water molecules and hydrated cations of the dissociated electrolyte molecules along the OHP, neutralized the negatively charged fraction of the surface (*i.e.* oxygen). Therefore, the remaining portion of the un-neutralized surface charge would be due to the surface cations. Since the surface cations sit below a surface dominated by oxygen atoms and are surrounded by oxygens in their primary coordination sphere this indicates that each of the positive regions created by these cations at the surface are isolated from each other. This suggests that the surface cations effectively function as independent point charges at the solid/aqueous interface.

Since Brown *et al.*'s[19] work demonstrated that hydrated anions are found only in the diffuse region (general solution) this indicates that they come from the dissociated electrolyte (LiCl, NaCl, KCl, and CsCl) and titrating acid or base solutions (*i.e.* H^+–Cl^-, Na^+–OH^-, *etc.*). The dissociated water molecules (H^+–OH^-) would most likely also provide another source of negatively charged ions. All these together would then be responsible for neutralizing the surface cations charge. Therefore, each of these ions would be electrostatically adsorbed above the hydrated cations at the OHP, in the diffuse region (general solution).

This suggests that the concentration of H^+ ions from the dissociated water molecules (*i.e.* H^+ and OH^-) and acid titrating solutions (*i.e.* H^+–Cl^-) are what is measured to obtain the materials pH_{PZC} below a pH = 7. Above a pH = 7, the titrant used would be a base, such as NaOH, which dissociates into Na^+ and OH^-. The anions from the electrolyte (LiCl, NaCl, KCl, and CsCl), base (*i.e.* NaOH) and dissociated water would then be adsorbed above the OHP to neutralize surface cations. This suggests that the H^+ ions which constitute the measured pH_{PZC} value are only from the dissociated water molecules. Therefore, the smaller source of H^+ ions most likely explains why a pH $\geq$ 7.0 is measured.

1.4 Adsorption models predicting point of zero charge

The mathematics for each model developed to predict PZC values are based on the concept of the change in Free Energy of the surface [eqn (1)][12] as protons ($H^{+)}$ and hydroxyls ($O–H^-$) adsorb onto the surface out of solution.

$$\Delta G^0 = \Delta G_{el} + \Delta G_{ch} \quad (1)$$

where: ΔG^0 = free energy at standard temperature and pressure, ΔG_{el} = electrical free energy, ΔG_{ch} = chemical free energy.

Eqn (1) can be rewritten in the manner of eqn (2) or (3) (ref. 12)

$$\Delta G^0 = \frac{2Z_H Z_O\ Ne^2}{\varepsilon_1 r} + \frac{2Z_H Z_O \nu\ Ne^2}{\varepsilon_2 r} + G_{ch} \quad (2)$$

where: Z_H = charge on a hydrogen (+1), Z_O = charge on an oxygen (−2), N = Avogadro's number, M = coordination number (*i.e.* number of bonds surrounding an atom)

$$\nu = Z_M/M$$

r = bond length between an oxygen and hydrogen (1.01 Å), L = M–O bond length

$$L = L + r$$

ε_1 = the effective dielectric constant of oxygen, ε_2 = the effective dielectric constant of hydrogen

$$\Delta G^0 = -2.3RT \log K \quad (3)$$

where: R = universal gas constant of, T = temperature (K°), K = equilibrium constant of the attached hydroxyls and hydrogens.

Multiple models were considered for use in this work. One important model considered was the Multisite Complexation (MUSIC) model developed by Heimstra *et al.*[21] Many of the other models available are essentially iterations of Heimstra *et al.*'s[21] basic concepts. The basis of these models is that all the adsorption sites at the surface behave as a single system. Therefor the equilibrium constant(s) (K) for the surface represents the value for the entire surface. In addition, the MUSIC model[21] incorporates different K values for metal-oxide and -hydroxide surfaces.

These models though do not fit the physical system determined by Brown *et al.*[19] They demonstrated that (1) the oxygen atoms are fully neutralized by water molecules and that the hydrated electrolyte cations, appear to neutralize the adsorbed water molecule's oxygen charge at the surface of the Stern layer. The remaining source of unresolved charge is from the surface cations which behave as separate point charge sources due to their position below the oxygen atoms. In addition, the multisite adsorption complex models cannot model complex metal-oxide and -hydroxide surface structures or phases in Region II, where the pH_{PZC} decreases below Region I. Therefore, they could not be used for the modelling objectives in this work.

The model which does treat each cation adsorption site as an individual point source was developed by Yoon *et al.*[12,21] They expanded the initial model developed by Parks,[16] incorporating the material's entire crystal structure and composition into their model. In addition, their model allows the calculation of a predicted point of zero charge (PPZC) for both simple and

complex metal-oxide and -hydroxide values. Finally, their model most closely resembles the physical system determined by Livey and Murray,[18] Brown *et al.*[19] and Leffler *et al.*[13]

To model the surface structure of a simple or complex metal-oxide/–hydroxide, it is necessary for each of the variables in the model to be a quantifiable parameter. These include physical structure factors and/or surface properties. In addition, the know structures of the material need to be identified. Multiple metal-oxides/hydroxides have multiple structures, such as mercuric oxide (HgO) which possess coordination numbers (C.N.) of both 2 and 6 (ref. 12 and 22–24) Therefore, the objectives of this work were to: (1) eliminate any non-structure factors used in Yoon *et al.*'s model eqn (2),[12] (2) identify, confirm and incorporate any unidentified physical parameters of the material (*i.e.* surface properties), (3) identify all the possible crystal structures and their structure factors at equilibrium, and (4) develop a method for applying the model to determine which is the most likely global surface structure present at its solid/aqueous interface.

2 Augmentation of the model used to determine surface structure and composition from its PZC

The crystal structure factors included in Yoon *et al.*'s[12] model are metal–oxygen bond length(s) (L), coordination number(s) (M), bond valence(s) (ν), metal oxidation state(s) (Z_M) and the fraction of Dangling surface bonds per metal cation (f_i) being modelled. The variable which is not a crystal structure factor is $L = L + 1.01$ Å. It is the average metal–oxygen bond length (L) (*i.e.* M^{2+}–O^{2-}) for each of the cations in the structure, with the addition of a hydroxyl (*i.e.* O–H^{1-}) bond length. This hydroxyl is formed when hydrogen ions (H^+) in solution adsorbs and/or bonds to oxygens bonded to the central cation. The reason O–H^{-1} ($r = 1.01$ Å) is not considered part of the bond length L is because it is not part of the primary coordination sphere surrounding the metal cation which is defined by its coordination number (M). Rather the adsorbed H^+ is considered part of the secondary coordination sphere which surrounds the primary coordination sphere. These consist of ligands that are attached to the ligands in the primary coordination sphere.[25] Since the H^+ is part of the secondary coordination sphere the O–H^- is a separate bond from the M^{2+}–O^{2-} bond and therefore their lengths cannot be added and treated as a single bond length.

To illustrate the effect of adding the hydroxyl's bond length to the average metal–oxygen bond length (L) in their model[12] it was found to shift the predicted pH_{PPZC} to a more basic value. An example of the use of this variable in their model with (L) and without (*i.e.* only L) comes from Table I in Yoon *et al.*'s[12] work. The experimental PZC value for SiO_2 is with a $pH_{PZC} = 1.80$. Using L and all the other structure factors in Table I[12] for SiO_2 in the model, a $pH_{PPZC} = -1.85$ is obtained. Replacing L with the structures average bond length L, results in a $pH_{PPZC} = -14.56$. Therefore, it appears that by using the extended bond length L in the model compensated for the lower pH_{PPZC} values predicted without it.

This variable (L) also poses a problem with regards to the findings of Leffler *et al.*[13] They determined that pH_{PZC} values shift toward significantly lower pH values as the surface M^{2+}–O^{2-} surface bonds expand at the anatase titania solid/aqueous interface in Region II.[13] This indicates that there is a physical parameter absent from Yoon *et al.*'s original model[12] that would perform the same function as the L variable and account for changes in surface bond lengths. Therefore, it was decided to remove the variable L from the model, replace it with the structures average bond length (L) and then determine the physical property not accounted for in the original model.

Leffler *et al.*[13] identified the property that might replace the L variable and account for the effect of changes in surface bond lengths effect on the materials PZC value. It is based on the knowledge that ionic/covalent bonds form an electric dipole which is defined by its dipole moment μ (Coulombmeters). As the ionic/covalent bond length expands/contracts its dipole moment increases/decreases, resulting in a shift in the ionic character of the bond. The ratio of an ionic/covalent bond's observed dipole moment (μ_o) with its ideal dipole moment ($\mu_I = 100\%$) provides the bond's percent ionic character ($I_{\%} = \mu_o/\mu_I$).[26]

Leffler *et al.*[13] identified the surface ionic/covalent bond(s) in Region I as having observed dipole moment(s) (μ_o) as they are smaller than the bulk structure bond(s) due to their shorter length.[27] Bulk structure bonds possess the maximum possible length(s) within the structure, giving them the greatest possible dipole moment(s). This identifies them as possessing the ideal dipole moment ($\mu_I = 100\%$). Therefore, in Region II, where the surface bonds expand toward those in the bulk structure,[27] this shifts the observed dipole moment(s) toward the ideal dipole moment. The result is that the surface bond's ionic character increases toward an ionic character ($I_{\%}$) = 100%.

Use of the bonds ionic content in the augmented model[12] is supported by work of Bickmore *et al.*[28] They presented the mathematical justification for a method incorporating a bonds ionic content into the modelling of the pK_a (acidity of a substance) value for solution monomers. Their work was then use by Mitchel[29] to augment the MUSIC model to predict PZC values for gibbsite ($Al(OH)_3$).

To determine if the ionic content of surface bonds can replace L in the model, the L variable was removed from Yoon *et al.*'s model[12] and replaced with L. The original equation [eqn (2)] was then rearranged to form eqn (4), where X represents the value of the possible variable that might replace L. Structure factors and PZC values for titania were used in eqn (4). These were $L = 1.969$ Å, oxidation state (Z_M) = +4, and the coordination number (M) = 6, which came from the example for TiO_2 in Table I in Yoon *et al.*'s work.[12] The PZC value used was determined by Leffler *et al.*[13] in Region I, where $pH_{PZC} \cong 7.17$, as it remains constant above an average diameter ≅29 nm. The value calculated from eqn (4) gave an $X = 0.6214$.

$$X = \frac{\mathrm{PZC} - 18.43}{f_i \times \left(\left(-53.12 \times \left(\frac{\nu}{L}\right)\right) + \left(\frac{1}{2} \times \log\left(\frac{2-\nu}{\nu}\right)\right)\right)} \quad (4)$$

where: Z_M = oxidation state of a cation, M = coordination number of cation, $\nu = Z_M/M$, L = Average cation–oxygen bond length (Å), f_i = fraction of Dangling surface bonds per metal cation (%)

To determine if $X = 0.6214$ is equivalent to Pauling's percent ionic content ($I_{\%}$), eqn (5) and values from Pauling's Electronegative Scale[30] were used to determine the ionic character for the Ti^{4+}–O^{2-} bond.

$$I_{\%} = 1 - \exp\left[-\left(\frac{(X_1 - X_2)^2}{4}\right)\right] \quad (5)$$

where:

$$X_{Ox} = 3.5$$

$$X_{Ti} = 1.5$$

The value determined from eqn (5) was $I_{\%} = 0.6321$. The difference between the calculated value X [eqn (4)] and Pauling's $I_{\%}$ is 0.0107 (1.69%), which indicates that the ionic character of the bond is one of the variables responsible for determining the surface's PZC value. Therefore, X was replaced with the variable for the ionic ch of the surface bond ($f_{I\%} = I_{\%}$) in eqn (4). Rearranging eqn (4) gave eqn (6). Eqn (5) is used to determine the ionic character of the bonds ($f_{I\%}$) for each atom in the structure in Region I. Eqn (6) constitutes the augmented Yoon *et al.* model[12] used in this work.

$$pH_{PPZC} = 18.43 - \left(\left(53.12 \times \sum_i^n f_{I\%} f_i \left(\frac{v}{L}\right)_i\right) - \frac{1}{2}\sum_i^n \left(f_{I\%} f_i \log\left(\frac{2-v}{v}\right)_i\right)\right) \quad (6)$$

where:

$$f_{I\%} = I_{\%}$$

The calculated value for $f_{I\%} = 0.6321$ for anatase titania was then used to model the pH_{PPZC} for anatase titania using eqn (6), along with the structure factors in Table I.[12] This resulted in a $pH_{PPZC} = 6.97$. This pH_{PPZC} value is within the error range (pH $= \pm 0.2$) of the Hanna pH meter used by Leffler *et al.*[13] to obtain their experimental PZC values. These results demonstrate that the ionic content of the bond is the correct physical property to replace L in the original Yoon *et al.* model.[12]

3 Development of the modelling method

3.1 Determination of surface structure in an aqueous environment

The method developed for this work is modelled after the approach used for the Rietveld Refinement method[31] used for determining the structure of a material's X-ray diffraction (XRD) pattern. The initial XRD pattern is obtained for a known phase. The composition and atomic positions are placed in a control file from which an XRD pattern is calculated. The program then calculates the differences between the experimental and modelled pattern. Each variable in the control file is then altered within the given parameters of each value, to calculate a pattern closest to the experimental pattern that is being modelled. The goodness of fit (R^2) determines how close the experimental and modelled patterns are. This same approach alters the modelled PZC values within their allowed physical parameters (*i.e.* bond lengths, composition, bond ionic content, and coordination number) until the difference between the two values is equal to or less than 0.5 pH units. When the model cannot converge, it indicates that the structure in the control file does not match the experimental XRD pattern. This is equivalent to the modelled pH_{PPZC} being greater than 0.5 pH units than the experimental pH_{PZC}.

The structure information used by Parks[32] and Yoon *et al.*[12] in their modelling work is for material not in an aqueous environment. When a metal-oxide or -hydroxide is placed in an aqueous environment, the global surface crystal structure and composition may not be the thermodynamically preferred phase present in the dominant species phase in the solution at its measured pH_{PZC} value. This might result in the surface structure and/or composition transforming to that of the dominant species phase in the solution at the pH_{PZC}.

To test this possibility, each of the phases presented in Yoon *et al.*'s work (Tables I–III)[12] were compared to the dominant species at their pH_{PZC} values, using their Pourbaix Diagrams.[33–37] In Table I[12] six of the phases were found not to be the dominant species phase at their pH_{PZC}. In Table II[12] two samples varied from the dominant species phase at the material's pH_{PZC} values. In some cases, both metal-oxides and their -hydroxide counterparts are stable in the same pH range. When this occurred, secondary information was consulted to identify the most likely surface structure at the material's pH_{PZC}. Once the dominant species phase was identified it replaced the phase modelled in Tables I–III.[12] Examples from Tables I–III[12] are presented in Sections 3.1.1–3.1.3. The remaining phases from Tables I and II not presented Tables 1 and 2 are included in the SI Section A. Explanations for how and why certain phases were replaced with the dominant species phase are presented after each table and for those tables contained in the SI Section A.

3.1.1 Table I dominant species

3.1.1.1 Magnesium hydroxide ($Mg(OH)_2$). Magnesium hydroxide is more thermodynamically stable than magnesium

Table 1 Dominant species present at each sample's pH_{PZC} in Table I[12,33–35]

Sample	Dominant species	Experimental point of zero charge (pH)
MgO	$Mg(OH)_2$	12.4
La_2O_3	$La(OH)_3$	10.4
ZrO_2	$Zr(OH)_4$	10.0–11.0
α-AlO(OH)	$Al(OH)_3$	7.7
γ- AlO(OH)	$Al(OH)_3$	7.5
Y_2O_3	$Y(OH)_3$	9.0

Table 2 Dominant species present at each sample's pH_{PZC} in Table II[12,33–37] with the presence of nonzero crystal field splitting effect

Sample	Dominant species	Experimental point of zero charge (pH)
$Fe(OH)_2$	$Fe(OH)_3$	12.0 ± 0.5
$Ni(OH)_2$	NiO	11.1
$Cu(OH)_2$	CuO	7.7

oxide (MgO)[35,38] in an aqueous environment. The Pourbaix diagrams present a pH stability range for $Mg(OH)_2$ from ≅9–16.[33–35] In the Pourbaix diagrams for magnesium, only $Mg(OH)_2$ is present in all the Eh-pH fields examined. Based on this information, it was determined that the surface of magnesium oxide most likely transforms to its hydroxide phase in an aqueous environment at its pH_{PZC} value.

3.1.1.2 Lanthanum hydroxide ($La(OH)_3$). When exposed to moisture at ambient temperature and pressure La_2O_3 rapidly transforms to $La(OH)_3$ making it the thermodynamically preferred phase[39]. This explains why $La(OH)_3$ is the dominant species in the Pourbaix diagrams[33–35] examined. Therefore, the experimental PZC value given for La_2O_3 in Table I[12] is the most likely surface structure of lanthanum hydroxide in an aqueous environment.

3.1.1.3 Zirconium hydroxide ($Zr(OH)_4$). According to multiple Pourbaix diagrams,[33–35] there are two stable dominant species present at a pH_{PZC} = 10–11,[12] these are ZrO_2 and $Zr(OH)_4$. While ZrO_2 is stable in an aqueous environment, the undoped meta-stable tetragonal phase (C.N. = 8) was used to model the pH_{PPZC} in Table 1.[12] Meta-stable tetragonal ZrO_2 phase though, rapidly transforms to its most stable form at ambient temperature and pressure, which is the monoclinic structure with a C.N. = 7.[40–42] The lower coordination number would shift the predicted value toward a lower pHppzc in this model [eqn (6)]. This is supported by the literature value for monoclinic zirconia of pH_{PZC} = 8.5,[43] which comes from a sample with a particle size of 0.1 μm, placing it within the material's Region I.[13,44]

The second dominant species in the Pourbaix diagrams examined was for zirconium hydroxide [$Zr(OH)_4$, ($ZrO_2 \cdot 2H_2O$)].[33–35] This phase has a C.N. = 8.[45] As the coordination number in the model [eqn (6)] increases, the predicted PZC value shifts towards a more basic pH_{PPZC}. Other PZC values measured for zirconium hydroxide are also in the range of pH = 10–11.[45,46] Therefore, the structure modelled in Table I[12] in the pH_{PZC} = 10–11 range is most likely zirconium hydroxide.

3.1.1.4 Aluminium hydroxide (γ – $Al(OH)_3$/α – $Al(OH)_3$: gibbsite). There are four phases of aluminium hydroxide, gibbsite, diaspore, boehmite, and bayerite.[47] The phase with the most stable free energy of these four aluminium hydroxides is gibbsite (hydrargillite).[35] The Eh–pH diagram for aluminium hydroxide also shows only the gibbsite structure in the pH range from pH = 4–11.[48] Therefore, the examples of diaspore (α-AlO(OH)) and Boehmite (γ-AlO(OH)) in Table I were not modelled as their surface structure had most likely transformed to the gibbsite phase.

3.1.1.5 Yttrium hydroxide ($Y(OH)_3$). Yttrium oxide (Y_2O_3), when placed in an aqueous environment, rapidly hydrates and transforms to yttrium hydroxide ($Y(OH)_3$).[49] This makes it the thermodynamically preferred structure in the presence of moisture. In addition, only yttrium hydroxide ($Y(OH)_3$) is present in the Pourbaix diagrams[33–35] examined and are present in a pH range of 6.5 to 16. Therefore, yttrium hydroxide was most likely the surface structure present in the aqueous environment at its pH_{PZC} = 9.0.

3.1.2 Table II dominant species. Three of the six phases in Table II[12] were not the dominant species phase at their pH_{PZC} values in an aqueous environment. Therefore, they were replaced with the dominant species phase present at the material's pH_{PZC}. Explanations for why these three phases were replaced are presented below Table 2.

3.1.2.1 Iron hydroxide ($Fe(OH)_3$). The Pourbaix diagrams[33–35] consulted indicate that $Fe(OH)_3$ is the dominant species at the pH_{PZC} value presented in Table II.[12] This is supported by the thermodynamic data, for the transformation equation: $4Fe(OH)_2 + O_2 + 2H_2O \Rightarrow 4Fe(OH)_3$ that gives a Gibbs free energy (ΔG) of −91.53 kJ mol^{-1}.[50] Therefore, it indicates that in an aqueous environment $Fe(OH)_2$ spontaneously transforms to $Fe(OH)_3$.

3.1.2.2 Nickel oxide (NiO). Until recently, the pH_{PZC} value for NiO had been identified as $Ni(OH)_2$ being the dominant species.[33–35] Recent work though has redefined the dominant species as NiO.[51,52] While the phase boundaries in these Pourbaix diagrams vary, they overlap from pH = 9.0 to 12.5. This range includes the most reliable basic value for NiO at a pH_{PZC} = 11.1.[53]

3.1.2.3 Copper oxide (CuO). Copper hydroxide ($Cu(OH)_2$) is a meta-stable phase which transforms to the stable CuO at ambient temperature and pressure in a basic aqueous solution (pH > 7).[54] Pourbaix diagrams for copper,[33–35] under these conditions, indicate that copper oxide (CuO) is the dominant stable species up to a pH ≅ 12.8. The most basic PZC value found in the literature is for a pH_{PZC} = 10.0,[55] which lies within this range of values. Therefore, the surface of the $Cu(OH)_2$ would most likely have transformed to CuO at a pH_{PZC} > 7.

3.1.3 Table III dominant species. Pourbaix diagrams could not be located for any of the complex metal oxides in Table III.[12] Therefore, secondary sources were consulted to confirm the structure factors. First, the most common oxidation states for these two cations are Al^{3+} and Si^{4+}.[22] In addition, all three of these structures have such low dissolution rates at ambient temperature and pressure they are essentially insoluble in acids and bases.[38,56] This suggests there is little chance of any significant surface dissolution, changing either the composition and/or structure in an aqueous environment during duration of the measurement of the materials pH_{PZC}.

While SiO_2 remains stable in this pH range [0–12.5],[33] aluminium oxide hydrates to its stable form $Al(OH)_3$.[57] An examination of the difference between the ionic radii for OH^{1-} and O^{2-} at coordination numbers of 4 and 6, determined that they are effectively equal.[22] Therefore, based on this information, the surface and bulk bond lengths for the Al–O sites, in

these three complex oxides, are the same as the hydroxide (*i.e.* Al–OH) in an aqueous environment at their pH_{PZC} values. Therefore, the surface Al^{3+} was modelled with an oxide bond (*i.e.* Al^{3+}–O^{2-}).

3.2 Modelling results

3.2.1 Table I. In Sections 3.1.1–3.1.3 the dominant species present at each material's pH_{PZC} were identified. Therefore, these were the phases modelled. Then, based on the results in Section 2, the most basic pH_{PZC} values were obtained after an extensive examination of the literature for each phase in Tables I–III[12] for use in the modelling work. The protocols developed by Leffler *et al.*[13] were used to assess the pH_{PZC} values chosen from the literature to minimize any possible differences between them and those in its Region I.[13]

Where the pH_{PZC} and pH_{PPZC} values were greater than pH = ±0.5, literature values for each phase's structure factors such as bond length and coordination number were examined. After identifying the structure factor(s) which varied from the information in Table I,[12] these different structure factor(s) for the material were replaced in the model. The final structure values, pH_{PZC} and pH_{PPZC} values presented in Table 1 are given in Table 4. Explanations for each phase where a structure factor and/or pH_{PZC} value was replaced are presented after Table 4. The phases in Table I, not included in Table 4 and their explanations are given in SI Material B.

3.2.1.1 Lanthanum hydroxide ($La(OH)_3$). While La_2O_3 has a C.N. = 6,[12] $La(OH)_3$ has a C.N. = 9 and an average bond length of L = 2.566 Å.[22] The most basic experimental PZC value found for $La(OH)_3$ is a pH_{PZC} = 12.40.[1] When the structure factors were placed in the model, it [eqn (6)] predicted a pH_{PPZC} = 12.90, with a difference of 0.5 pH units.

3.2.1.2 Yttrium hydroxide ($Y(OH)_3$). The structure of $Y(OH)_3$ has a C. N. = 9 (ref. 62) and an average bond length L = 2.43 Å.[22] The most basic pH_{PZC} available in the literature is for a pH = 12.8.[63] The pH_{PPZC} = 12.83, a difference of only 0.03 pH units.

3.2.2 Table II. The same process carried out in Section 3.2.1 was followed for the Table II[12] structures. Results of this modelling work are presented in Table 5. All six metal-oxides in Table II diverged from the structure information presented by Yoon *et al.*[12] Explanations for how these model's structure factors were resolved are presented after Table 5. The phases in Table II, not included in Table 5 and their explanations are given in SI Material B.

3.2.2.1 Iron(III) hydroxide ($Fe(OH)_3$). The dominant species found on the Pourbaix diagram for iron is $Fe(OH)_3$. The common coordination number for iron is six coordinated,[12] with an average surface bond length of L = 2.09 Å in an aqueous environment. This is longer than the bond length of 1.99 Å measured using XRD for the dry powder of $Fe(OH)_3$.[64] When these structure factors, which included an oxidation state (Z_M) = +3 were placed in the model [eqn (6)] a pH_{PPZC} = 11.65, a difference of 0.35 pH units from pH_{PZC} = 12.0 ± 0.5 of the experimental value was obtained.

3.2.2.2 Nickel oxide (NiO). Using the structure factors provided by Yoon *et al.*[12] resulted in a pH_{PPZC} = 13.68, more than two pH units above the experimental value of pH_{PZC} = 11.10. Based on the most current Pourbaix diagrams,[51,52] NiO was identified as the dominant species, not $Ni(OH)_2$, which ruled out changing the oxidation state structure factor. This indicates another structure factor might vary from the bulk structure.

This was found to be the case. It was determined that while the bulk crystal structure of NiO has a coordination number of 6, work by Che and Bonneviot[65] demonstrated that at the [1 0 0] crystal face of NiO the surface atom, Ni^{2+}, has a square pyramidal symmetry (C.N. = 4). Since NiO has a simple rock salt cubic structure,[69] each crystal lattice face is identical, and all the Ni^{2+} atoms are four coordinated.[70] They also found that corners and edges present lower coordination numbers of 3 and 4. Therefore, replacing C.N. = 6 with a C.N. = 4 and calculating the average bond length for this value (L = 1.91 Å)[22] resulted in a pH_{PPZC} = 11.04, only 0.06 pH units different than the experimental value.

3.2.2.3 Copper oxide (CuO). Copper oxide is the thermodynamically stable structure with its most basic pH_{PZC} = 10.0.[66] Therefore, its oxidation state is +2. Using the bulk structure factors from Yoon *et al.*[12] (C. N. = 4) resulted in a pH_{PPZC} = 11.91. Reducing the C.N. value to 2 results in a pH_{PPZC} = 5.87, 4.03 pH units below the materials PZC value. Modelling work by Maimaiti *et al.*[67] using Density Functional Theory (DFT) predicted a C.N. = 3 for its surface structure with an average L = 2.024 Å.[68] Using these values in the model resulted in a pH_{PPZC} = 10.01, a difference of 0.01 pH units.

3.2.3 Table III. The final set of examples is for three complex metal-oxide alumina silicates. Surface structure modelling of these three phases confirms the surface structure factors[71] presented in Yoon *et al.*[12] are correct. These values are presented in Table 6.

Each of the pH_{PPZC} values calculated using eqn (6), are presented in Table 7. The pH_{PPZC} values all fall within the range of experimental values presented in Yoon *et al.*'s work[12,58,59] and within ±0.6 pH units of the average of these experimental values. Therefore, no changes to the structure factors values were considered necessary for these three aluminosilicate samples. These results also confirm that the surface structure and composition are not affected by an aqueous environment.[38,56]

A comparison of the two experimental pH_{PZC} values[58,59] though suggests that surface composition and structure may have varied from the bulk structure. These variations in the surface may have been due to processing work (*i.e.* grinding) exposing different cleavages with slightly different compositions or contamination.[71] Based on the model's sensitivity to slight changes in each of the structure factors used to determine a pH_{PPZC}, one or all these factors might explain the larger variation than pH = ± 0.5 from some of the materials average pH_{PZC} in Table 7.

3.2.4 Analysis of hematite (α-Fe_2O_3) surface structure transformation over time. The prior modelling examples were taken from Yoon *et al.*'s[12] work for single measurements obtained a one point in time. This example is an analysis of work by Lutzenkirchen *et al.*[14] on the measured changes in pH_{PZC} for

the same hematite surface over time. It illustrates how this method can be used to model structural changes responsible for shifting the measured pH_{PZC} values.

The measured pH_{PZC} values were for the surface of a 10 × 20 mm^2 hematite crystal electrode. The initial pH_{PZC} value was measured right after its surface had been freshly fractured. Following each measurement, the electrode was then cleaned with ethanol and milliQ-water. The sample was then aged in water for 30-minutes intervals, eight times (240 min. total) at 600 °C. Dividing up the total period from 0 minutes to 240 minutes, gave intervals of 80 minutes between each PZC measurement. What they found was a significant shift in the PZC values of the hematite electrode's surface, from the initial $pH_{PZC} = 3.85$ to their steady state value of $pH_{PZC} = 8.80$.

The most basic pH_{PZC} found in the literature is from work done by Klein Wolterink *et al.*[72] Their hematite powder was aged for 480 minutes (8 h) at 120 °C under 1.2 atmospheres. The extended aging time resulted in a $pH_{PZC} = 9.80$. This value is most likely closest to the final equilibrium PZC for the hematite surface in Region I.[13] The equilibrium structure for hematite in Region I comes from the work by Jones *et al.*[73] They determined that the most stable surface structure on the most stable crystal face [0 1 1] of hematite exhibited a five coordinated Fe^{3+} atom. When placed into eqn (6), the model converged to a $pH_{PPZC} = 9.92$, only 0.12 pH units above Klein Wolterink *et al.*'s[72] measured PZC value. While the final value measured by Lutzenkirchen *et al.*[14] was more than 1.1 pH units below Klein Wolterink *et al.*'s.[72] Therefore, the value obtained by Klein Wolterink[72] was placed in Fig. 2, as it appears to be the equilibrium PZC value for hematite.

The first step in modelling the hematite electrode's surface was to determine the initial coordination value for the F^{3+} atoms on the freshly fractured hematite electrode. This was obtained from work by Schottner *et al.*[74] They used adsorbed carbon monoxide (CO) to determine the oxygen coordination for the surface Fe^{3+} atoms of a freshly fractured pristine hematite surface. Their results determined that the Fe^{3+} atoms had a coordination number of three oxygen atoms surrounding them. Work by Jones *et al.*[73] identified a bond length for the three coordinated Fe^{3+} of $L = 1.88$ Å. Placing these structure factors into the model [eqn (6)] gave a $pH_{PPZC} = 3.89$, only 0.04 pH units different from the experimental value presented in Fig. 2 and `s C1 and C2 [SI Section C]. The model [eqn (6)] also confirmed the experimental findings by Schottner *et al.*[74] that the surface for a pristine, newly fractured surface has an Fe^{3+} atom with a C.N. = 3 (ref. 12, 73 and 74) in an aqueous environment.

The critical information explaining how the surface structure changed also comes from Lutzenkirchen *et al.*'s[14] work. Their examination of the freshly fractured electrode revealed that the surface had two doubly coordinated hydroxyl groups present. This suggests that the oxygen of these doubly coordinated hydroxyls might have been sitting in oxygen vacancies adjacent to but not bonded to the Fe^{+3} atoms. As the PZC values shifted, they found that the number of surface hydroxyls decreased from two to one. This suggests that an oxygen atom from each of the doubly coordinated hydroxyls bonded with Fe^{3+} atoms. It is supported by the increased roughness of the surface, which suggests it was due to a newly formed Fe^{3+}–O^{2-} bonds extending upward from the surface.

To determine the most reasonable bonding sequence responsible for the change in PZC values [Fig. 2] two different models were executed. Since hematite is known to exhibit 4 coordinated sites,[75] the first model was for a bonding sequence of Fe^{3+} sites shifting in a sequence of C.N. = 3 => C.N. = 4, then 4 => C.N. = 5. These results are presented in Fig. 3 and Table C1 [SI Section C]. The second bonding sequence modelled is for the C.N. = 3 going directly to a C.N. = 5. These results are presented in Fig. 4 and Table C2 [SI Section C].

Fig. 3 and 4 were compared with Fig. 2. The results in Fig. 2 and 4 demonstrate a parallel shift in their curves over time. Therefore, these results suggest the sequence responsible for the shift in PZC values is presented in Fig. 4 and Table C2 [SI Section C] where the C.N. = 3 => C.N. = 5.

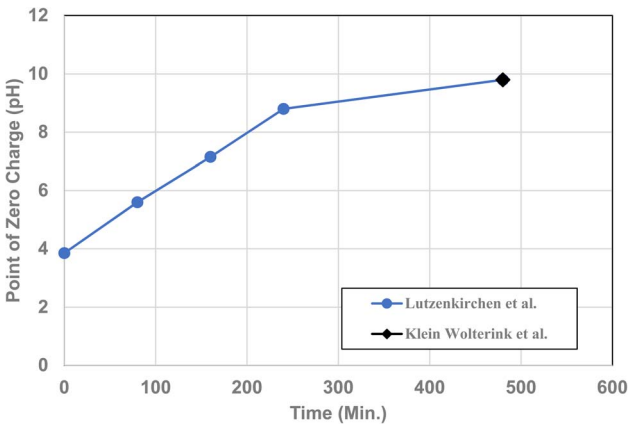

Fig. 2 The point of zero charge for the hematite surface after aging against the time interval at which it was measured.[14] The data point at 480 min. is for the equilibrium PZC value in Region I.[72]

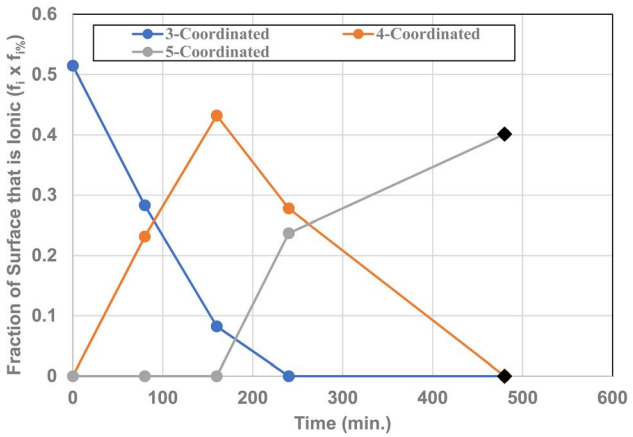

Fig. 3 The bonding sequence of changes in the coordination number of oxygen around the Fe^{3+} central cation (C.N. = 3 => C.N. = 4 => C.N. = 5). The fraction of the surface which is ionic ($f_i \times f_{|\%}$) is plotted against the time at which it was measured. The values are presented in Table C1 [SI Section C].

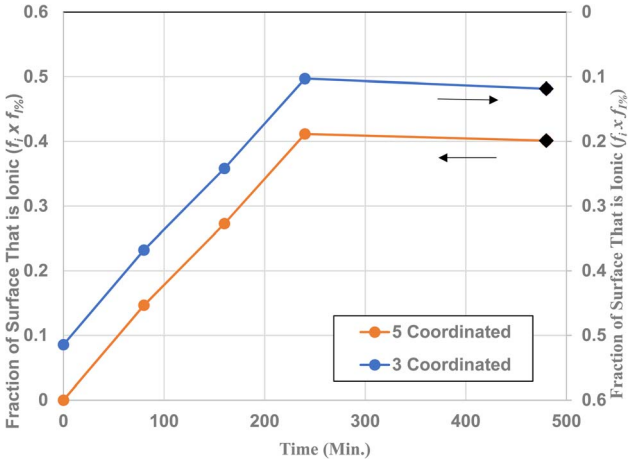

Fig. 4 The bonding sequence of changes in the coordination number of oxygen around the Fe^{3+} central cation (C.N. 3 => C.N. 5). The fraction of the surface which is ionic ($f_i \times f_{i\%}$) is plotted against the time at which it was measured. The values are presented in Table C2 [SI Section C].

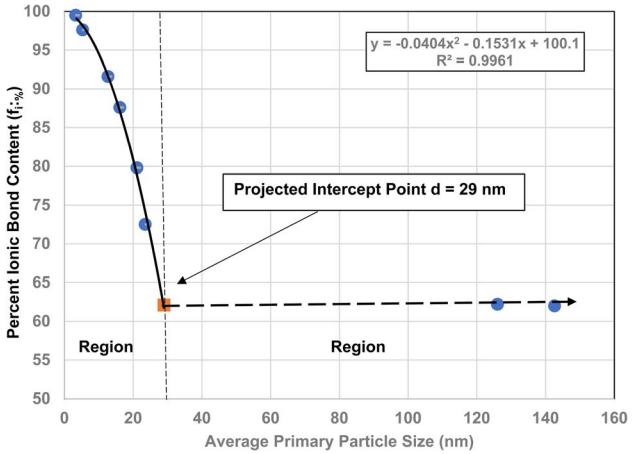

Fig. 5 Modelled bond ionic character of anatase titania against their average primary particle diameters from literature values.[13,76]

The argument for choosing the Fig. 4 sequence is that the two double hydroxyls identified in the surface structure[14] were probably sitting in the oxygen vacancies next to each Fe^{3+} atom. Therefore, the simplest and most expedient path available to drive surface energy to its lowest value [18] would be for the double hydroxyl oxygens to bond directly to the Fe^{3+} atoms. Whereas the C.N. = 3 => C.N. = 4 => C.N. = 5 would most likely have been reflected in a different set of shifts in PZC values over time and might result in a higher surface energy during this transition.

3.3 Determination of the anatase titania bond ionic character in regions I and II

In Section 2 the bond ionic content in Region I for anatase titania was calculated using eqn (4), the structure inputs from Table I[12] and the pH_{PZC} from work by Leffler *et al.*[13,76] Their work also demonstrated that in Region II, surface bond lengths (*i.e.* Band gaps) expand with decreasing particle size. Therefore, it was necessary to obtain the average surface bond length as the average primary particle size decreased. This would allow use of the correct surface bond length (L) be used in eqn (4) as well as the samples pH_{PZC}.

This was accomplished by obtaining the average bond length within the bulk structure for anatase titania. Work by Pantaleone *et al.*[77] provided both the average bond length for anatase titania at the surface [$L \cong 1.8$ Å–1.9 Å] and within the bulk structure [$L \cong 2.1$ Å]. Assigning the bond length [$L = 1.986$] from Yoon *et al.*'s[12] Table I for anatase titania to the surface in Region I at $d = 29$ nm, and $L \cong 2.1$ Å at $d = 3.30$ nm[76] the simple equation for a line was fitted to these two points [eqn (7)].

$$y = -0.0051x + 2.1168 \quad (7)$$

The bond lengths calculated using eqn (7) are presented in Table C1 [SI Materials C], along with the bond ionic content [eqn (4)] pH_{PZC}, and average primary particle diameter[13,76] for each sample.

Surface bond ionic content was then plotted against their average primary particle diameter and is presented in Fig. 5. What is most interesting is that the bond ionic content of particle ($d = 3.30$ nm) where superconductivity occurred[76] has an $I_{\%} = 99.5\%$, indicating surface bonds were essentially purely ionic. The calculated bond length [eqn (4)] where $I_{\%} = 100\%$ for the particle where superconductivity occurred is at $L = 2.115$ Å, a difference of only 0.71%. An interesting note, while the surface bond lengths were calculated using the equation for a line, the curve for the percent ionic content presents the same form as the pH_{PZC} values in Region II,[13] a polynomial.

Lastly, the bulk bond length can also be used to determine the lowest pH_{PZC} where the surface bonds are fully ionic. This is accomplished by using all the structure factors in Region I, save the average surface bond length (L) and the bond ionic content determined from Pauling's electronegative table and eqn (4). To obtain the pH_{PZC} value where surface bonds are fully ionic, $f_{\%I} = 1.0$ and $L =$ Average bulk structure bond length (2.115 Å).

4 Discussion

Prior to this work, most of the models predicting PZC values used the central premise, that all the adsorption sites at the surface interacted with each other. This required determining global equilibrium constant(s) for different surfaces using various methods. Work by Livey and Murray,[18] Brown *et al.*[19] and Leffler *et al.*[13] though demonstrated that surface oxygens dominate the surface and are fully neutralized by water molecules in the Stern layer. Then the hydrated cations from the electrolyte at the outer Helmholtz plane neutralize the charge on the water's oxygen adsorbed on to the surface.

The anions from the dissociated electrolyte, titrant and water molecules are most likely responsible for neutralizing the cations at the surface, adsorbing above the OHP over the surface cations in the Diffuse Region (general solution). The PZC value below a $pH_{PZC} \leq 7$ is determined by measuring the H^+ ions from

Table 3 Dominant species present at each sample's pH_{PZC} in Table II[12,33–35,58,59]

Sample	Dominant species	Experimental point of zero charge (pH)	Experimental point of zero charge (pH)
Kyanite	Kyanite	7.9	6.9
Andalusite	Andalusite	7.2	5.2
Sillimanite	Sillimanite	6.8	6.0

the dissociated acid titrant and water. In the basic region (*i.e.* $pH_{PZC} \geq 7$) the $O\text{–}H^-$ from the dissociated base and water molecules are what most likely neutralize the surface cations. Only the H^+ ion concentration from dissociated water molecules is what is measured to determine the material's PZC value.

Prior to this work, modelling PZC values for simple and complex metal-oxides and –hydroxides were carried out under the assumption that their bulk and surface structures were identical.[12,32] Based on Pourbaix diagrams of each simple and complex metal-oxides or -hydroxides suggests they may possess a structure which, at times, is independent of their bulk phase when exposed to an aqueous environment at different pH values. Therefore, from the literature and modelling results presented in Tables 1–7, and SI Tables A1–D1, it has been demonstrated that in an aqueous environment the surface structure being modelled can vary significantly from the bulk structure.

There are several modelling methods that look at material systems surfaces. The first is the Molecular Dynamic (MD)[78] modelling method which focuses on the motion of molecules and atoms within a system. Work by Brown *et al.*'s[19] and Leffler *et al.*'s[13] on the interface structure though shows they possess a stable structure at the solid/aqueous interface. This is because surface molecules and ions are electrostatically adsorbed (*i.e.* attached). In addition, no literature using this method was ever located that provided the needed surface structure and composition at the solid/water interface. Therefor this method found not to be applicable in determining the stable surface structure and composition at its solid/aqueous interface.

A second modelling method of a surface's structure and composition is the Density Functional Theory (DFT). This method is a quantum mechanical method for modelling stable multi-body systems, making it ideal for determining possible surface structures in an aqueous environment.[79] Were the solid/aqueous structures not stable, measurements such as reproducible zeta potential curves that converge at a zeta potential of 0 mV where the particle move through an electric field at differing pH values and electrolyte concentration would not be possible. In addition, the literature searches for surface structures all produced models using DFT. These were for copper oxide (CuO),[68,80] and hematite (α-Fe_2O_3)[81] and were used as possible surface structures which varied from the materials bulk structure at their PZC in the model [eqn (6)].

Work by Leffler *et al.*[13,76] found that the surface bonds in Region I all have the essentially the same bulk indirect band gap

Table 4 Structure parameters, pH_{PZC} and $pH_{PPZC,}$ values for the metal-oxide/-hydroxide examples in Table I[12,30]

Dominant species	C.N.	Z_M	L (Å)	$f_{i\%}$ (%)	f_i	$=f_i \times I_{\%}$	Exp. pH_{PZC}	Cal. pH_{PPZC}	Ref.
$Mg(OH)_2$	6	+2	2.06	0.7335	1	0.7335	12.0	11.87	12 and 60
$La(OH)_3$	9	+3	2.566	0.7631	1	0.7631	12.40	12.90	12, 1, 22 and 61
$Zr(OH)_4$	8	+4	2.26	0.6680	1	0.6680	10–11	10.422	12, 45 and 46
$Y(OH)_3$	9	+3	2.43	0.7335	1	0.7335	12.80	12.83	12, 62 and 63

Table 5 Structure parameters for metal-oxides/hydroxide samples in Table II[12,30] with the presence of nonzero crystal field splitting effect

Dominant species	C.N.	Z_M	L (Å)	f_i (%)	$I_{\%}$	$=f_i \times I_{\%}$	Exp. pH_{PZC}	Cal. pH_{PPZC}	Ref.
$Fe(OH)_3$	6	+3	2.09	1.0	0.5145	0.5145	12.0 ± 0.5	11.65	12 and 64
NiO	4	+2	1.91	1.0	0.5145	0.5145	11.1 ± 0.4	11.04	12, 22 and 65
CuO	3	+2	2.01	1.0	0.4727	0.4727	10.0	9.95	12, 66, 67 and 68

Table 6 Structure parameters for kyanite, andalusite, and sillimanite in Table III.[12] The value below the number of bonds is the percentage of the total number of bonds for that atom in the structure

Sample	(f_i) $Si^{(IV)a}$	(f_i) $Al^{(IV)a}$	(f_i) $Al^{(V)a}$	(f_i) $Al^{(VI)a}$	L $Si^{(IV)a}$ (Å)	L $Al^{(IV)a}$ (Å)	L $Al^{(V)a}$ (Å)	L $Al^{(VI)a}$ (Å)
Kyanite	16 (25.0%)			48 (75.0%)	1.625			1.91
Andalusite	16 (26.7%)		20 (33.3%)	24 (40.0%)	1.62		1.84	1.93
Sillimanite	16 (28.6%)	16 (28.6%)		24 (42.8%)	1.61	1.77		1.91

[a] Coordination number.

Table 7 Calculated structure factors and pH_{PZC} values for kyanite, andalusite and sillimanite for Table III[12,30,58,59]

Sample	$I_{\%}$	$=f_i \times I_{\%}$ Si–$O^{(IV)a}$	$=f_i \times I_{\%}$ Al–$O^{(IV)a}$	$=f_i \times I_{\%}$ Al–$O^{(VI)a}$	$=f_i \times I_{\%}$ Al–$O^{(VI)a}$	Exp. pH_{PZC}	Exp. pH_{PZC}	Avg. Exp. pH_{PZC}	Calc. pH_{PPZC}
Kyanite	Si = 0.5145 Al = 0.6321	0.128			0.4742	6.9	7.9	7.4	7.58
Andalusite	Si = 0.5145 Al = 0.6321	0.137		0.211	0.253	5.2	7.2	6.2	6.79
Sillimanite	Si = 0.5145 Al = 0.6321	0.135	0.181		0.270	5.6	6.8	6.2	5.74

[a] Coordination number.

value (~3.2 eV) for anatase titania. This indicates that they are all essentially the same length above a particle diameter of ≅29 nm. In addition, the material's bond ionic content ($f_{I\%}$) determined using eqn (4) (ref. 30) and presented in Fig. 5 are constant in Region I. Further, these values ($f_{I\%}$) were determined to be essentially equal to what is obtained using Pauling's eqn (5) and his table of electronegative values[30] in Region I for TiO_2. Therefore, determination of a material's surface structure needs to be done using the pH_{PZC} value in Region I, as all the structure factors needed are available.

Once the surface structure in Region I is determined, eqn (4) can be employed to determine the ionic content of the surface bonds ($f_{I\%}$) in Region II, using the method described in Section 3.3. This makes it possible to model the bond ionic content for the surface bonds for each average primary particle in Region II. At present, though the limitation for determining the ionic character of the surface bonds in Region II using this method can only be applied to simple metal-oxides and -hydroxides.

Based on the findings in this work it has been demonstrated that the augmented model developed in this paper is applicable to both simple and complex metal-oxides and -hydroxides, but only in Region I. At present the modelling of surface bond ionic content in Region II is restricted to simple metal-oxides and -hydroxides, as demonstrated in Fig. 5 and Table D1 in SI Section D. The reason for this is that at present it is not known if all the metal oxide bonds for different cations in complex metal-oxides and hydroxides expand linearly. Future work will focus on how each of the bonds for complex metal-oxides and hydroxides change in Region II.

Based on the methodology developed for this work, it is evident that it is not a stand-alone method. To obtain reliable results the user must be able draw from multiple areas such as thermodynamics, crystallography, X-ray diffraction, electrochemistry, Density Functional Theory modelling, *etc.* In addition, Leffler *et al.*[13] developed a protocol for correctly measuring PZC values with a minimum of error. This method should be incorporated into the measurement scheme for the sample. Therefore, it is critical that when using this method all these factors be considered for the surface structure under test.

5 Conclusions

This work demonstrates a completely new method for modelling the global surface structure, and composition at the solid/aqueous interface for both simple and complex metal-oxides and -hydroxides in Region I using the material's PZC. In Region II it has been shown that as the materials PZC decreases with its average primary particle diameter, the surface bond ionic content for simple metal-oxides and – hydroxides can be measured directly. To accomplish this the model [eqn (2)] developed by Yoon *et al.*'s[12] was augmented [eqn (6)] to determine both the structure factors for the primary coordination sphere of each cation and their bond ionic content using Pauling's electronegative table and eqn (5).[30]

A method was then developed to apply Yoon *et al.*'s[12] augmented model [eqn (6)] to obtain the global surface

structure and composition at the solid/aqueous interface of simple and complex metal-oxides and -hydroxides in Region I.

This method requires knowledge of:

1. The correct dominant species at the material's pH_{PZC}.

2. All the possible phases formed by this dominant species.

3. The most basic pH_{PZC} value for the surface structure available either experimentally or in the literature.

4. The most thermodynamically stable phase present in an aqueous environment where multiple phases might be present in the same aqueous environment, and

5. All the possible bulk and surface structure information of the dominant species phase at the material's pH_{PZC} from both experimental and/or modelling methods such as DFT.

Once this information has been acquired, each of the possible structures at the materials PZC values are entered into model until it converges to its measured experimental PZC value.

What makes this model and method so useful, is that it can be applied in multiple fields such as catalysis, flotation, electrochemistry for battery and capacitor development, remediation of contaminated regions, confirming surface models (*i.e.* DFT) in an aqueous environment and the treatment of clothing (*i.e.* dying). It can also be used to predict a materials PZC value when the average primary particle size is in its Region I for complex metal-oxides and -hydroxides over a series of compositions. This is also the only experimental means at present of determining metal-oxides and hydroxides global surface structure, composition and bond ionic content of each cation in an aqueous environment. Lastly, the PZC measurement is economical and SI and multiple analytical tests on the material to model the surface are readily available in the literature.

Future work will focus on developing this modelling method to determine the structure, composition and changes in the bond ionic content of each cation–oxygen bond in complex metal-oxides and -hydroxides in Region II. This will allow its application to complex nanoscale metal-oxides and -hydroxides with an average primary particle diameter that are under test in Region II. Lastly, an examination of whether this modelling method can be applied to phases under test using cyclic voltammetry. The reason for investigating this possibility is because the shift in voltage values translates to changing pH values at the surface of the material across this range.

Conflicts of interest

The authors declare that they have no known competing financial interests or personal relationships that could have appeared to influence the work reported in this paper.

Data availability

All data used in this work will be available on request to any interested party.

Supplementary information (SI) is available. See DOI: https://doi.org/10.1039/d6ra00388e.

Acknowledgements

SLS thank NEUCORSE for partial support of this research.

References

1 S. R. Rao and J. Leja, *Surface Chemistry of Froth Flotation, Second Edition, Volume 1*, Fundamentals, Springer Science + Business Media, LLC, New York. 2004.

2 W. Wu and E. V. Shevchenko, The surface science of nanoparticles for catalysis: electronic and steric effects of organic ligands, *J. Nanopart. Res.*, 2018, **20**, 1–14.

3 A. M. Munshi, R. N. Singh, M. Kumar and J. P. Singh, Effect of nanoparticle size on sessile droplet contact angle, *J. Appl. Phys.*, 2008, **103**, 0843315.

4 H. Zhang, R. L. Penn, R. J. Hamers and J. F. Banfield, Enhanced Adsorption of Molecules on Surfaces of Nanocrystalline Particles, *J. Phys. Chem. B*, 1999, **103**(22), 4656–4662.

5 S. N. Guilhen, T. Watanabe, T. T. Silva, S. Rovani, J. T. Marumo, J. A. S. Tenorio, O. Masek and L. Goulart de Araujo, Role of Point of Zero Charge in the Adsorption of Cationic Textile Dye on Standard Biochars from Aqueous Solutions: Selection Criteria and Performance Assessment, *Recent Progress in Materials*, 2022, **4**(2), 1–20.

6 S. Slesinska, P. Galek, J. Menzel, S. W. Donne, K. Fic and A. Ptatek-Mielczarek, Fundamentals and Implication of Point of Zero Charge (PZC) Determination for Activated Carbons in Aqueous Electrolytes, *Adv. Sci.*, 2024, **11**, 2409162–2409172.

7 T. Megyes, S. Balint, T. Grosz, T. Radnai and I. Bako, The Structure of aqueous sodium hydroxide solutions: A combined solution x-ray diffraction and simulation study, *J. Chem. Phys.*, 2008, **128**(4), 044501–044512.

8 H. Jiang, Z. Song, M. Ling and S. Du Z. Yang, FTIR studies of recombinant human graulocyte-macrophage colony-stimulating factor in aqueous solutions: secondary structure, disulfide reduction and thermal behavior, *Biochim. Biophys. Acta*, 1996, **1294**(2), 121–128.

9 A. M. Noval, D. Nishio, T. Kuruma and S. Hayakawa, Coordination and structure of Ca(II)-acetate complexes in aqueous solution studied by combination of Raman and XAFS spectroscopies, *J. Mol. Struct.*, 2018, **1161**, 512–518.

10 L. Guo, R. H. Colby, M. Y. Lin and G. P. Dado, Micellar structure changes in aqueous mixtures of nonionic surfactants, *J. Rheol.*, 2001, **45**(5), 1223–1243.

11 H. Yang and Y. Lim, Solution Structure Determination of Four *Diploptera punctata* Allatostatins by NMR Spectroscopy and Molecular Modeling, *Bull. Korean Chem. Soc.*, 2005, **26**(5), 845–848.

12 R. H. Yoon, T. Salman and G. Donnay, Predicting Points of Zero Charge of Oxides and Hydroxides, *J. Colloid Interface Sci.*, 1979, **70**(3), 483–493.

13 M. Leffler, A. Mirich, J. Fee, S. March and S. L. Suib, Part I: determination of a structure/property transformation mechanism responsible for changes in the point of zero

charge of anatase titania with decreasing particle size, *RSC Adv.*, 2024, **14**, 30543–30565.
14 J. Lutzenkirchen, F. Heberling, F. Suplijika, T. Preocanin, N. Kallay, F. Johann and E. P. J. Weisser, Structure – charge relationship – the case of hematite (0 l 0), *Faraday Discuss.*, 2015, **180**, 55–79.
15 A. Auer, X. Ding, A. S. Bandarenka and J. Kunze-Liebhauser, The Potential of Zero Charge and Electrochemical Interface Structure of Cu(111) in Alkaline Solutions, *J. Phys. Chem. C*, 2021, **125**, 5020–5028.
16 P. A. Di, S. Ikeda, G. Marci, B. Ohtani and L. Palmisano, Transition metal doped TiO_2: physical properties and photocatalytic behavior, *Int. J. Photoenergy*, 2001, **3**, 171–176.
17 M. Suchanek, E. Niewiara, K. Wilkosz and W. W. Kubiak, Nanopowders of Yttria-Stabilized Zirconia Doped with Rare Earth Elements as Adsorbents of Humic Acids, *Materials*, 2019, **12**, 3915–3930.
18 D. T. Livey and P. Murray, Surface Energies of Solid Oxides and Carbides, *J. Am. Ceram. Soc.*, 1956, **39**(11), 363–372.
19 M. A. Brown, Z. Abbas, A. Kleibert, R. G. Green, A. Goel, S. May and T. M. Squires, Determination of Surface Potential and Electrical Double-Layer Structure at the Aqueous Electrolyte-Nanoparticle Interface, *Phys. Rev. X*, 2016, **6**, 011007.
20 R. Chang, *Chemistry*, Random House, New York, 1st edn, 1981.
21 T. Heimstra, W. H. Van Riemsdijk and G. H. Bolt, Multisite Proton Adsorption Modeling at the Solid/Solution Interface of (hydr)oxides: A New Approach: Model description and evaluation of intrinsic reaction constants, *J. Colloid Interface Sci.*, 1989, **133**(1), 91–104.
22 R. D. Shannon, Revised effective ionic radii and systematic studies of inter-atomic distances in halides and chalcogenides, *Acta Crystallogr.*, 1976, **A32**, 751–767.
23 L. R. Merte, M. S. Jorgensen, K. Pussi, J. Gustafson, M. Shipilin, A. Schaefer, C. Zang, J. Rawle, C. Nicklin, G. Thornton, R. Linday, B. Hammer and E. Lundgren, Structure of the SnO2(110) - (4 × 1) Surface, *Phys. Rev. Lett.*, 2017, **119**(9), 1–6.
24 O. W. L. Carter, Y. Xu and P. J. Sadler, Minerals in biology and medicine, *RSC Adv.*, 2021, **11**(4), 1939–1951.
25 L. V. A. Hale and N. K. Szymczak, Hydrogen Transfer Catalysis beyond the Primary Coordination Sphere, *ACS Catal.*, 2018, **8**, 6446–6461.
26 M. Tuckerman, E. Vitz, J. W. Moore, J. Shorb, X. Prat-Resina, T. Wendorff, A. Hahn and R. J. Lancashire, Contributors, Electronegativity and Dipole Moment, https://chem.libretexts.org/@go/page/41350.2020.
27 C. Q. Sun, L. Li, B. K. Tay and H. Huang, An extended 'quantum confinement' theory: Surface-coordination imperfection modifies the entire band structure of a nanosolid, *J. Phys. D: Appl. Phys.*, 2001, **34**(24), 3470–3479.
28 B. R. Bickmore, C. J. Tadanier, K. M. Rosso, W. D. Monn and D. L. Eggett, Bond-valence methods for pK_a prediction: critical reanalysis and a new approach, *Geochem. Cosmochim. Acta*, 2004, **68**(9), 2025–2042.
29 S. C. Mitchell, *An Improved MUSIC Model for Gibbsite*, Brigham Young University, Masters, 2005.
30 L. Pauling, *The Nature of the Chemical Bond*, Cornell University Press, Ithaca New York, 3rd edn, 1960.
31 R. A. Young and D. B. Wiles, *National Bureau of Standards Special Publication 567*, National Bureau of Standards, Washington D. C., 1980, 567, 143 – 162.
32 G. A. Parks, The Isoelectric Points of Solid Oxides, Solid Hydroxides, and Aqueous Hydroxo Complex Systems, *Chem. Rev.*, 1965, **65**(2), 177–198.
33 D. G. Brookins, *Eh-pH Diagrams for Geochemistry*, Springer – Verlag Berlin Heidelberg, 1st edn, 1988.
34 N. Takeno, *Atlas of Eh – pH Diagrams, Geological Survey of Japan Open File Report No. 419*, National Institute of Advanced Industrial Science and Technology Research Center for Deep Geological Environments, 2005.
35 M. Pourbaix, *Atlas of Electrochemical Equilibria in Aqueous Solutions*, J. A. Translator Franklin, National Association of Corrosion Engineers, Houston TX, 1974.
36 F. Basharat, U. A. Rana, M. Shahid and M. Serwar, Heat treatment of electrodeposited NiO films for improved catalytic water oxidation, *RSC Adv.*, 2015, **5**, 86713–86722.
37 L.-F. Huang, M. J. Hutchison, Jr. R. J. Santucci, J. R. Scully and J. M. Rondinelli, Improved Electrochemical Phase Diagrams from Theory and Experiment: The Ni – Water System and Its Complex Compounds, *J. Phys. Chem. C*, 2017, **121**(18), 9782–9789.
38 R. C. Weast, D. R. Lide, M. J. Astle and W. H. Beyer, *Handbook of Chemistry and Physics*, CRC Press, Boca Ratan, Florida, 70th edn, 1990.
39 P. Fleming, R. A. Farrell, J. D. Holmes and M. A. Morris, The Rapid Formation of $La(OH)_3$ from La_2O_3 Powders on Exposure to Water Vapor, *J. Am. Ceram. Soc.*, 2010, **93**(4), 1187–1194.
40 S. Xie, E. Iglesta and A. T. Bell, Water-Assisted Tetragonal-to-Monoclinic Phase Transformation of ZrO_2 at Low Temperature, *Chem. Mater.*, 2000, **12**(8), 2442–2447.
41 F. Zhang, P. J. Chupas, S. L. A. Liu, J. C. Hanson, W. A. Caliebe, P. L. Lee and S. W. Chan, In situ Study of the Crystallization from Amorphous to Cubic Zirconium Oxide: Rietveld and Reverse Monte Carlo Analyses, *Chem. Mater.*, 2007, **19**(13), 3118–3126.
42 P. Southon, *Structural Evolution during the Preparation and Heating of Nanophase Zirconia Gels*, Ph. D. Thesis, University of Technology, Sydney Australia, 2000.
43 G. A. El, Measurement of the diffuse double-layer between zirconia and alumina, *J. Appl. Phys.*, 1999, **86**(10), 5894–5897.
44 M. Leffler, *Chemistry Dept.*, University of Connecticut, Unpublished results, 2021.
45 D. Petrescu, L. Velciu and C. Bucur, *Antimony Removal from Aqueous Solutions Using Zirconium Hydroxide*, International Atomic Energy Agency, Nuclear, 2016.
46 A. S. C. Chen, G. M. Lewis and L. Wang, *Arsenic Removal from Drinking Water by Adsorptive Media EPA Demonstration Project at Golden Hills Community Services District in Tehachapi, CA Final Performance Evaluation Report, National Risk Management Research Laboratory*, Office of Research and

Development, U. S. Environmental Protection Agency, Cincinnati, Ohio 45268, 2010.
47 G. A. Parks, Free Energies of Formation and Aqueous Solubilities of Aluminium Hydroxides and Oxide Hydroxides at 25°C, *Am. Mineral.*, 1972, **57**, 1163–1189.
48 V. G. Krivovichev, M. V. Charykova and A. V. Vishnevsky, The Thermodynamics of Selenium Minerals in Near-Surface Environments, *Minerals*, 2017, **7**(10), 188.
49 P. Lindqvist-Reis, Hydration of the Yttrium (III) Ion in Aqueous Solution. An X-ray Diffraction and XAFS Structural Study, *J. Phys. Chem. B*, 2000, **104**(2), 402–408.
50 R. C. Weast, D. R. Lide, M. J. Astle and W. H. Beyer, *Handbook of Chemistry and Physics*, CRC Press, Boca Ratan, Florida, 70th edn, 1990.
51 F. Basharat, U. A. Rana, M. Shahid and M. Serwar, Heat treatment of electrodeposited NiO films for improved catalytic water oxidation, *RSC Adv.*, 2015, **5**, 86713–86722.
52 L.-F. Huang, M. J. Hutchison, Jr. R. J. Santucci, J. R. Scully and J. M. Rondinelli, Improved Electrochemical Phase Diagrams from Theory and Experiment: The Ni – Water System and Its Complex Compounds, *J. Phys. Chem. C*, 2017, **121**(18), 9782–9789.
53 G. A. Parks, The Isoelectric Points of Solid Oxides, Solid Hydroxides, and Aqueous Hydroxo Complex Systems, *Chem. Rev.*, 1965, **65**(2), 177–198.
54 Y. Cudennec and A. Lecerf, The transformation of $Cu(OH)_2$ into CuO, revisited, *Solid State Sci.*, 2003, **5**(11–12), 1471–1474.
55 H. Chang, C. S. Jwo, C. J. Lo, T. T. Tsung, M. J. Kao and H. M. Lin, Rheology of CuO Nanoparticle Suspension Prepared by ASNSS, *Rev. Adv. Mater. Sci.*, 2005, **10**, 128–132.
56 Y. Zhang, D. J. Rimstidt, Y. Huang and C. Zhu, Kyanite far from equilibrium dissolution rate at 0-22°C and pH of 3.5 – 7.5, *Acta Geochim.*, 2019, **38**, 472–480.
57 T. Shirai, h. Watanabe, M. Fuji and M. Takahashi, *Structural Properties and Surface Characteristics on Aluminum Oxide Powders*, Nagoya Institute of Technology Ceramic Research Annual Report, 2009, vol. 9, pp. 23–31.
58 J. J. Smolik, E. Harman and D. W. Fuerstenau, Surface characteristics and flotation of aluminosilicate, *Trans. AIME*, 1967, **235**, 367–375.
59 H. S. Choi, and J. H. Oh, *Surface properties and floatability of kyanite and andalusite, Jour. Min*, Met. Inst., Japan, 1965, 81(927), pp. 614–620.
60 J. X. Lin and L. Wang, Adsorption of dyes using magnesium hydroxide-modified diatomite, *Desalination Water Treat.*, 2009, **8**(1–3), 263–271.
61 J. M. Trillo, M. D. Alba, M. A. Castro, A. Munoz, J. Poyato and M. M. Tobias, Local Environment of Lanthanum Ions in Montmorillonite Upon Heating, *Clay Miner.*, 1992, **27**(4), 423–3.
62 T. Guner, A. Kus, M. Ozcan, A. Genc, H. Sahin and M. M. Demir, Green fabrication of lanthanide –doped hydroxide-based phosphors: $Y(OH)_3$:Eu^{3+} nanoparticles for white light generation, *Beilstein J. Nanotechnol.*, 2019, **10**, 1200–1210.
63 V. A. Hackley and S. G. Malghan, The surface chemistry of silicon nitride powder in the presence of dissolved ions, *J. Mater. Sci.*, 2004, **29**, 4420–4430.
64 K. Shinoda, E. Matsubara, A. Muramatsu and Y. Waseda, Local Structure of Ferric Hydroxide $Fe(OH)_3$ in Aqueous Solution by the Anomalous X-ray Scattering and EXAFS Method, *Mater. Trans.*, 1994, **35**(6), 394–398.
65 M. Che and L. Bonneviot, Role of oxide surface in coordination chemistry of transition metal ions in catalytic systems, *Pure Appl. Chem.*, 1988, **60**(8), 1369–1378.
66 H. Chang, C. S. Jwo, C. J. Lo, T. T. Tsung, M. J. Kao and H. M. Lin, Rheology of CuO Nanoparticle Suspension Prepared by ASNSS, *Rev. Adv. Mater. Sci.*, 2005, **10**, 128–132.
67 Y. Maimaiti, M. Nolan and S. D. Elliott, Reduction mechanisms of the CuO (1 1 1) surface through surface oxygen vacancy formation and hydrogen adsorption, *Phys. Chem. Chem. Phys.*, 2014, **16**(7), 3036–3046.
68 A. K. Mishra, A. Roldan and N. H. de Leeuw, CuO Surfaces and Co 2 Activation: A Dispersion-Corrected DFT+U Study, 2016 Dispersion-Corrected DFT+U Study, *J. Phys. Chem. C*, 2016, **120**(4), 2198–2214.
69 C.-C. Diao, C.-Y. Huang, C.-F. Yang and C.-C. Wu, Morphological, Optical, and Electrical Properties of p-type Nickel Oxide Thin Films by Nonvacuum Deposition, *Nanomaterials*, 2020, **10**(4), 636–641.
70 R. W. Cairns and E. Ott, X-Ray Studies of the System Nickel – Oxygen – Water. I. Nickelous Oxide and Hydroxide, *J. Am. Chem. Soc.*, 1933, **55**(2), 527–533.
71 C. M. Koretsky, D. A. Sverjensky and N. Sahai, A model of surface site types on oxide and silicate minerals based on crystal chemistry: Implications for surface site types and densities, multi-site adsorption, surface infrared spectroscopy, and dissolution kinetics, *Am. J. Sci.*, 1998, **298**, 349–438.
72 W. J. K. Klein, L. K. Koopal, M. A. Cohen Stuart and W. H. Van Riemskijk, Surface charge regulation upon polyelectrolyte adsorption, hematite, polystyrene sulfonate, surface charge regulation Theoretical calculations and hematite-poly(styrene sulfonate) system, *Colloids Surf., A*, 2006, **291**, 13–23.
73 F. Jones, A. L. Rohl, J. B. Farrow and W. van Bronswijk, Molecular modeling of water adsorption on hematite, *Phys. Chem. Chem. Phys.*, 2000, **14**, 3209–3216.
74 L. Schottner, A. Nefedov, C. Yang, S. Heissier, Y. Wang and C. Woll, Structural Evolution of α-Fe_2O_3 Surfaces Under Reduction Conditions Monitored by Infrared Spectroscopy, *Front. Chem.*, 2019, **7**(451), 1–12.
75 E. Wasserman, J. R. Rustad, A. R. Felmy, B. P. Hay and J. W. Halley, Ewald methods for polarizable surfaces with application to hydroxylation and hydrogen bonding on the (012) and (001) surfaces of α-Fe_2O_3, *Surf. Sci.*, 1997, **385**(2 – 3), 217–239.
76 M. Leffler, J. Fee, S. March, Y. Wu and S. L. Suib, Part II: Superconductivity Observed in Magnetically Separated Nanoscale Anatase Titania at Ambient Temperature and Pressure in an Aqueous Environment at its Point of Zero Charge, *RSC Adv.*, 2024, **14**, 30317–30335.

77 S. Pantaleone, F. Pellegrino, V. Maurino, M. Corno, P. Ugliengo and L. Mino, Disclosing the true atomic structure of {0 0 1} facets in shape-engineered TiO_2 anatase titania nanoparticles, *J. Mater. Chem. A*, 2024, **12**, 4325–4332.

78 *Molecular Dynamics*, Wikipedia, https://en.wikipedia.org/wiki/Molecular_dynamics.

79 *Density Functional Theory*, Wikipedia, https://en.wikipedia.org/wiki/Density_functional_theory.

80 Y. Maimaiti, M. Nolan and S. D. Elliott, Reduction mechanisms of the CuO (1 1 1) surface through surface oxygen vacancy formation and hydrogen adsorption, *Phys. Chem. Chem. Phys.*, 2014, **16**(7), 3036–3046.

81 N. Naveas, R. Pulido, C. Marini, J. Hernandez-Montelongo and M. M. Silvan, First-principles calculations of hematite (α-Fe_2O_3) by self-consistent DFT+U+V, *iScience*, 2023, **26**(2), 1–17.